The EMBO Journal Vol. 21 No. 17 pp. 4680–4690, 2002

Discrimination between mono- and trimethylated cap structures by two isoforms of *Caenorhabditis elegans* eIF4E

Hiroshi Miyoshi[1], Donard S.Dwyer[2], Brett D.Keiper, Marzena Jankowska-Anyszka[3], Edward Darzynkiewicz[4] and Robert E.Rhoads[5]

Departments of Biochemistry and Molecular Biology and [2]Psychiatry, Louisiana State University Health Sciences Center, Shreveport, LA 71130-3932, USA and Departments of [3]Chemistry and [4]Biophysics, University of Warsaw, 02-093 Warsaw, Poland

[1]Present address: Genomics Research Institute, Utsunomiya University, Utsunomiya-Shi, 321-8505, Japan

[5]Corresponding author
e-mail: rrhoad@lsuhsc.edu

Primitive eukaryotes like *Caenorhabditis elegans* produce mRNAs capped with either m^7GTP or $m_3^{2,2,7}$GTP. *Caenorhabditis elegans* also expresses five isoforms of the cap-binding protein eIF4E. Some isoforms (e.g. IFE-3) bind to m^7GTP–Sepharose exclusively, whereas others (e.g. IFE-5) bind to both m^7GTP– and $m_3^{2,2,7}$GTP–Sepharose. To examine specificity differences, we devised molecular models of the tertiary structures of IFE-3 and IFE-5, based on the known structure of mouse eIF4E-1. We then substituted amino acid sequences of IFE-5 with homologous sequences from IFE-3. As few as two changes (N64Y/V65L) converted the cap specificity of IFE-5 to essentially that of IFE-3. Molecular dynamics simulations suggested that the width and depth of the cap-binding cavity were larger in IFE-5 than in IFE-3 or the N64Y/V65L variant, supporting a model in which IFE-3 discriminates against $m_3^{2,2,7}$GTP by steric hindrance. Furthermore, the affinity of IFE-5 (but not IFE-3) for $m_3^{2,2,7}$GTP was reversibly increased when thiol reagents were removed. This was correlated with the formation of a disulfide bond between Cys-122 and Cys-126. Thus, translation of $m_3^{2,2,7}$GTP-capped mRNAs may be regulated by intracellular redox state.

Keywords: *Caenorhabditis elegans*/cap recognition/ molecular dynamics/*trans*-splicing/ 2,2,7-trimethylguanosine

Introduction

Initiation of protein synthesis proceeds by progressive assembly of initiation complexes, each stage catalyzed by a different set of initiation factors (Hershey and Merrick, 2000). Recruitment of mRNA to the 43S initiation complex in eukaryotes requires the eIF4 factors, which include the 25 kDa cap-binding protein eIF4E. Alterations in eIF4E levels and activity have a profound effect on cell growth and phenotype, presumably due to the differential recruitment of mRNAs specifically required for cell growth and cell cycle progression (De Benedetti and Harris, 1999).

The tertiary structure of mouse eIF4E-1 was solved by X-ray crystallography (Marcotrigiano *et al*., 1997) and that of yeast eIF4E by NMR spectroscopy (Matsuo *et al*., 1997). The binding of m^7GDP results from the stacking of the purine ring between Trp-56 and Trp-102 (using the mouse numbering), formation of H-bonds between N1 and N2 of m^7G and Glu-103, van der Waals interactions between the ribose moiety and Trp-56, and ionic interactions of the α- and β-phosphate oxygen atoms with Arg-157 and Lys-162. Addition of one methyl group at the N2 position of m^7G has little effect on cap binding to mammalian eIF4E, but addition of a second methyl group, to form 2,2,7-trimethylguanine ($m_3^{2,2,7}$G), markedly decreases binding (Darzynkiewicz *et al*., 1988; Carberry *et al*., 1990; Cai *et al*., 1999).

Two types of capped RNAs exist in eukaryotic cells. The primary transcripts for both mRNAs and small nuclear RNAs (snRNAs) are modified to form a 5′–5′ GpppN linkage, which is subsequently methylated in the nucleus to yield m^7GpppN (Varani, 1997). The cap of snRNAs is further methylated in the cytosol at N2 of m^7G, forming $m_3^{2,2,7}$GpppN (Mattaj, 1986). These methylations are dependent upon the binding of Sm proteins to form U-type small nuclear ribonuclear protein complexes (snRNPs) and are the signal for import of snRNPs into the nucleus (Hamm *et al*., 1990; Gorlich and Mattaj, 1996). The trimethylated cap structure is recognized by Snurportin1, a receptor for spliceosomal mRNPs that utilizes the importin β pathway for nuclear import (Huber *et al*., 1998). The strong preference of most eIF4Es for m^7G- versus $m_3^{2,2,7}$G-containing caps ensures that mRNAs rather than snRNAs are recruited to the translational machinery.

An exception to this paradigm is the acquisition of $m_3^{2,2,7}$G-containing caps by mRNAs through the process of *trans*-splicing, in which a 22 nucleotide spliced leader is transferred from the 5′-end of an snRNA to an acceptor site in the 5′ end of the pre-mRNA (Blumenthal, 1998). As a result, the original m^7G-containing cap is replaced by the $m_3^{2,2,7}$G-containing cap (van Doren and Hirsh, 1990). *Trans*-splicing of mRNA has been most studied in primitive eukaryotes like the nematode *Caenorhabditis elegans* (Zorio *et al*., 1994), but it also occurs in more complex chordate species (Vandenberghe *et al*., 2001). In *C.elegans*, the majority of mRNAs are *trans*-spliced. Both m^7G- and $m_3^{2,2,7}$G-capped mRNAs are found in the cytosol of *C.elegans* and are translated on polyribosomes (Liou and Blumenthal, 1990).

The fact that the well-studied eIF4Es of higher eukaryotes strongly prefer m^7G- to $m_3^{2,2,7}$G-capped mRNAs, yet *C.elegans* translates both types of mRNAs, led us to examine the eIF4E of *C.elegans* (Jankowska-Anyszka *et al*., 1998; Keiper *et al*., 2000). Surprisingly, five eIF4E isoforms are expressed in *C.elegans*, named IFE-1 to

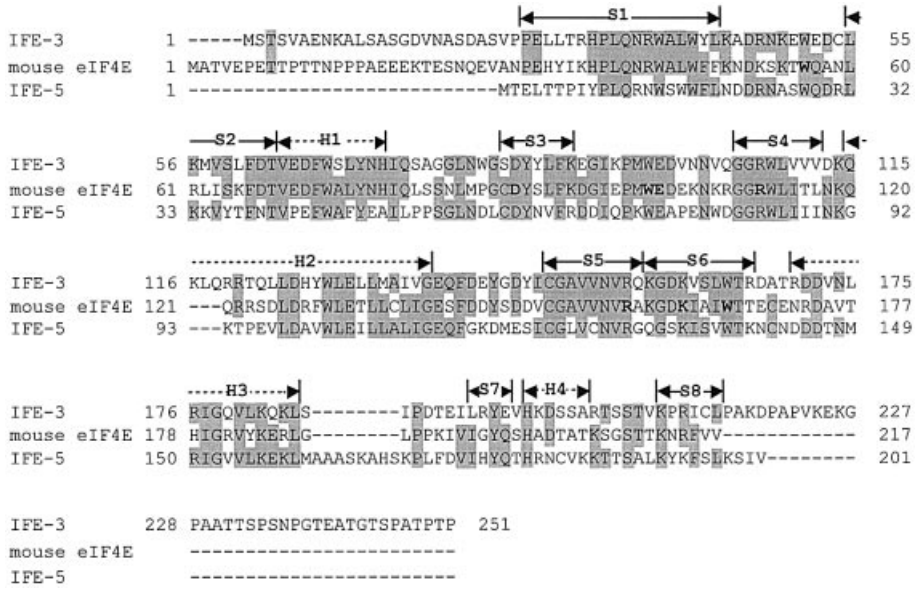

Fig. 1. Sequence comparisons between *C.elegans* IFE-3, mouse eIF4E and *C.elegans* IFE-5. Amino acid sequences were deduced from the cDNA sequences of IFE-3 (Jankowska-Anyszka *et al*., 1998), mouse eIF4E (Altmann *et al*., 1989) and IFE-5 (Keiper *et al*., 2000). Alignment was performed using the CLUSTAL W algorithm (version 1.8; http://www.ddbj.nig.ac.jp). Shading indicates identical residues. Secondary structure elements are designated as follows: S1, β-sheet 1; S2, β-sheet 2; H1, α-helix 1; H2, α-helix 2; etc. Amino acid residues that contact the cap in mouse eIF4E are shown in bold.

IFE-5. IFE-3 is the most homologous to mammalian eIF4E-1, is retained on m^7GTP–Sepharose but not $m_3^{2,2,7}$GTP–Sepharose, and is the only IFE that is essential for viability. IFE-4 has the same cap specificity, but is not essential. By contrast, two isoforms with closely related amino acid sequences, IFE-1 and IFE-5, are retained on both m^7GTP–Sepharose and $m_3^{2,2,7}$GTP–Sepharose. IFE-2, while not retained on $m_3^{2,2,7}$GTP–Sepharose, is nonetheless prevented from binding to m^7GTP–Sepharose by $m_3^{2,2,7}$GTP. IFE-1, -2 and -5 are partially redundant for viability, but at least one isoform is required. IFE-1 is expressed only in the gonad of maturing worms and plays an essential role for spermatogenesis in both males and hermaphrodites (Amiri *et al*., 2001).

In the present study, we have examined the structural basis for differences in cap discrimination among the IFE proteins. Such knowledge may give insight into the biological roles of the five IFE proteins of *C.elegans*, as well as the multiple eIF4E isoforms found in other organisms (Browning *et al*., 1987; Rychlik *et al*., 1987; Wakiyama *et al*., 1995; Gao *et al*., 1998; Myers *et al*., 2000). We find that changing just two amino acid residues can alter the cap discrimination of IFE-5 to resemble that of IFE-3. Based on dynamic tertiary structure models, we propose that this change results from a reduction in the average size of the cap-binding cavity. Unexpectedly, the cap discrimination of IFE-5 is reversibly changed by the formation of a disulfide bond between two Cys residues.

Results

Rationale and approach for determining the basis for cap discrimination

It is possible that a small subset of amino acid residues is responsible for the difference in cap specificity of the two classes of *C.elegans* eIF4E isoforms. Our broad strategy was to choose a representative of each eIF4E class, IFE-3 and IFE-5, interchange amino acid residues, and examine the specificity of cap recognition. One way to choose candidates for discriminatory amino acid residues is to examine regions that are likely to be in close proximity to the bound cap structure. Unfortunately, the tertiary structure has not been solved for any of the IFE proteins. However, the co-crystal structure of mouse eIF4E with m^7GDP has been solved and can serve as a template for model building of the IFE proteins.

Amino acid sequence alignment shows that mouse eIF4E is more similar to IFE-3 than to IFE-5 (Figure 1), in agreement with the calculated sequence identities (47% versus 41%) and the strong preference of both mammalian eIF4E and IFE-3 for m^7G-containing caps (Jankowska-Anyszka *et al*., 1998; Cai *et al*., 1999). Importantly, there is a high degree of sequence identity between mouse eIF4E and both IFE-3 and IFE-5 in the β-sheets identified by X-ray crystallography (s1, s3, etc.). We approximated the tertiary structures for IFE-3 and IFE-5 by homology modeling to the mouse eIF4E structure (Dwyer, 1996, 2001; Figure 2). After energy minimization, the root-mean-square deviations are 2.2 and 1.1 Å, respectively. The residues homologous to Trp-56 and Trp-102 of mouse eIF4E, which 'sandwich' the guanine ring, are Trp-51 and Trp-97 in IFE-3, and Trp-28 and Trp-74 in IFE-5.

The similarity of the IFE-3 and IFE-5 models (Figure 2), coupled with a knowledge of where the amino acid sequences deviate (Figure 1), allowed us to choose amino acid sequences that were likely to be involved in cap discrimination. The loop connecting β-sheets 1 and 2, referred to as the 1–2 loop, forms one side of the cap-binding pocket and could contribute side chains that determine specificity. The 3–4 loop, connecting β-sheets 3 and 4, forms the other side of the cap-binding pocket. It

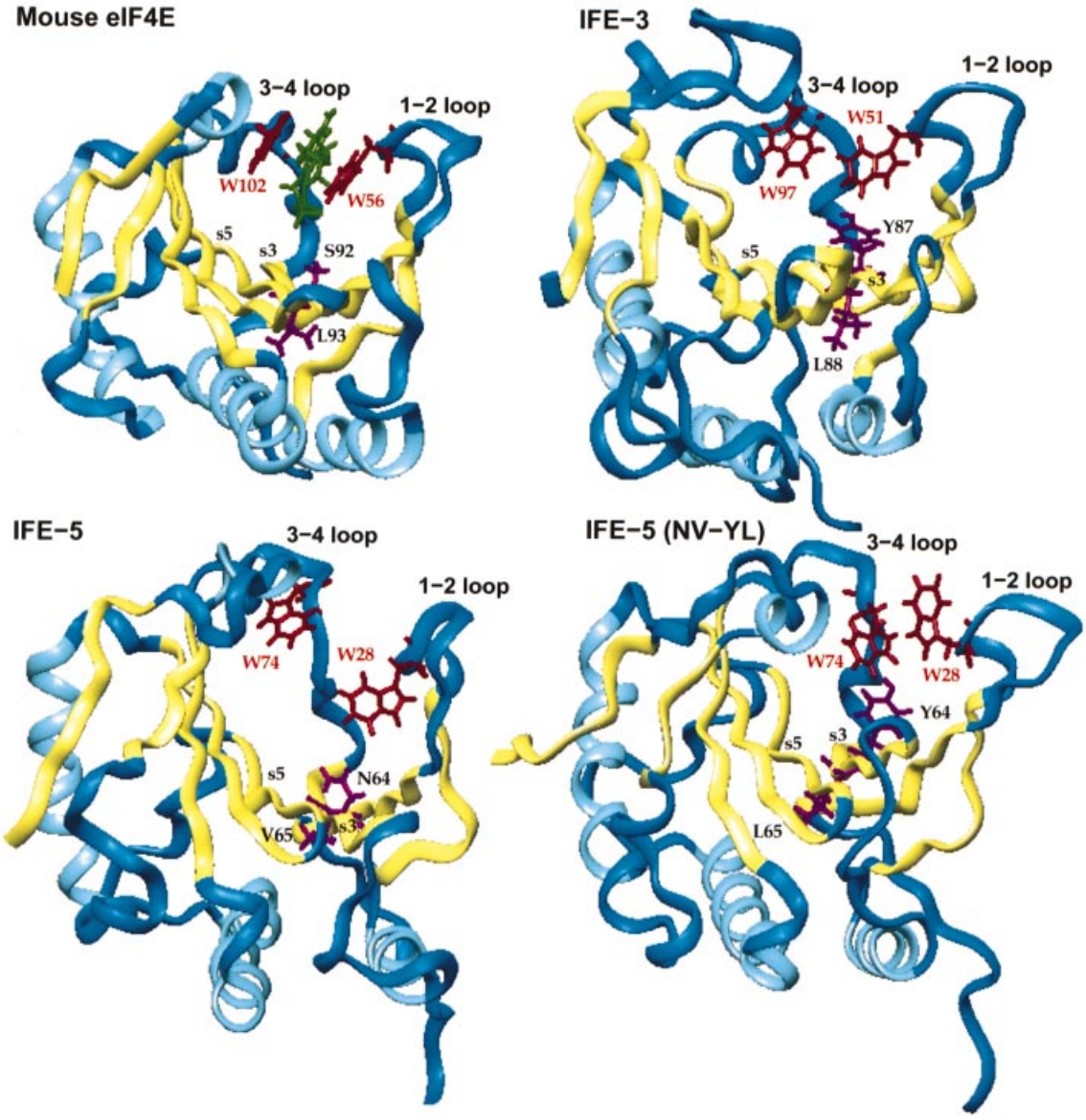

Fig. 2. Molecular models of IFE-3, IFE-5 and the NV-YL variant of IFE-5 in comparison with the crystal structure of mouse eIF4E. The figure was produced with the graphics interface of the Insight II software. N-terminal amino acid residues homologous to those truncated from mouse eIF4E prior to X-ray crystallography are not shown. The position of m^7GDP is shown in the mouse eIF4E structure. The structures of IFE-3, IFE-5 and IFE-5(NV-YL) were obtained from equivalent time points in MD simulations and are intended to show dynamic aspects of the binding site rather than the minimized structures. Selected amino acid side chains are shown in different colors and labeled in upper case letters using the one-letter code. Secondary structure elements (β-sheets in yellow, loops in dark blue, α-helices in light blue) are labeled in lower case letters, e.g. β-sheet 3 is 's3', etc. Loops connecting β-sheets are labeled 1–2 loop, etc. IFE structures are oriented the same as mouse eIF4E.

also contains a Glu residue homologous to Glu-103 in mouse eIF4E, which forms H-bonds with the N1 and N2 protons of m^7G; these protons are absent in $m_3^{2,2,7}G$. The loops are, therefore, attractive sites for modification.

Replacement of amino acid sequences in IFE-5 with homologous sequences from IFE-3

In variant 1–2 loop, the 1–2 loop in IFE-5 is replaced by the equivalent sequence from IFE-3 (Figure 3). This loop contains one of the two Trp residues sandwiching the cap guanine. In variant 3–4 up, the upstream (N-terminal) half of the 3–4 loop is replaced together with part of β-sheet 3, whereas in variant 3–4 down, the downstream (C-terminal) half of this same loop is replaced. This stretch of amino acids includes the other Trp residue sandwiching the m^7G. In other variants, the entire 3–4 loop is replaced (3–4 loop), or various types of 1–2 and 3–4 loop substitutions are combined (1–2 & 3–4 up, 1–2 & 3–4 down, and 1–2 & 3–4 loop). Finally, the upstream portion of the 3–4 loop is dissected with more selective substitutions (variants N-Y, V-L, NV-YL, DDIQPK-EGIKPM and QPK-KPM).

Qualitative testing of variants using affinity chromatography

IFE-5 variants were initially screened qualitatively for cap specificity by measuring their capture from *Escherichia coli* lysates on columns of either m^7GTP– or $m_3^{2,2,7}GTP$–

```
                    S1          S2      H1          S3          S4
IFE-5 wt        10 PLQRNWSWWFLNDDRNASWQDRLKKVYTFNTVPEFWAFYEAILPPSGLNDLCDYNVFRDDIQPKWEAPENWDGGRWLIII 89
1-2 loop        10 ...........KADRNKEWED.................................................... 89
3-4 up          10 ..................................................YLFKEGIKPM.............. 89
3-4 down        10 ....................................................MWEDVNNVQ........ 89
3-4 loop        10 ..................................................YLFKEGIKPMWEDVNNVQ........ 89
1-2 & 3-4 up    10 ...........KADRNKEWED.............................YLFKEGIKPM.............. 89
1-2 & 3-4 down  10 ...........KADRNKEWED.....................................MWEDVNNVQ........ 89
1-2 & 3-4 loop  10 ...........KADRNKEWED.............................YLFKEGIKPMWEDVNNVQ........ 89
N-Y             10 ..................................................Y..................... 89
V-L             10 ..................................................L..................... 89
NV-YL           10 ..................................................YL.................... 89
DDIQPK-EGIKPM   10 ..............................................EGIKPM.............. 89
QPK-KPM         10 ..............................................KPM.............. 89
IFE-3           10 PLQNRWALWYLKADRNKEWEDCLKMVSLFDTVEDFWSLYNHIQSAGGLNWGSDYYLFKEGIKPMWEDVNNVQGGRWLVVV 89
```

Fig. 3. Amino acid substitutions in IFE-5. Variants, named on the left, were constructed by substituting the indicated sequences of IFE-3 into the homologous positions of IFE-5. Letters in bold indicate amino acid residues that are conserved between IFE-3 and IFE-5.

Sepharose, followed by elution with m^7GTP or $m_3^{2,2,7}GTP$, respectively (Figure 4). In this qualitative assay, it is not possible to distinguish between proteins that are more highly expressed in soluble form and those with enhanced cap-binding activity; this distinction is made by measuring cap affinities of purified IFEs using the fluorescence-quenching assay (see below). Rather, the qualitative assays served to guide the construction of IFE-5 variants that showed a change in the relative binding to m^7GTP–Sepharose versus $m_3^{2,2,7}GTP$–Sepharose compared with wild-type (wt) IFE-5.

As reported previously (Jankowska-Anyszka *et al.*, 1998), IFE-3 is retained on m^7GTP–Sepharose (Figure 4A, lane M under IFE-3) but not $m_3^{2,2,7}GTP$–Sepharose (lane T). This indicates high selectivity for m^7G-containing caps, i.e. a 'mono-specific' IFE. By contrast, IFE-5 is retained both by m^7GTP–Sepharose (Figure 4A, lane M under IFE-5) and, to a lesser extent, by $m_3^{2,2,7}GTP$–Sepharose (lane T). This is the behavior of a 'dual-specific' IFE.

Comparing wt IFE-5 to several variants for relative binding to m^7GTP–Sepharose versus $m_3^{2,2,7}GTP$–Sepharose, variant 3–4 up appears to show the highest selectivity for m^7GTP (Figure 4A). The variant 3–4 down, on the other hand, binds $m_3^{2,2,7}GTP$–Sepharose more efficiently than wt IFE-5, despite similar binding to m^7GTP–Sepharose. Thus, it displays lower selectivity for m^7GTP than IFE-5. These results suggest that a discriminatory element (favoring m^7GTP over $m_3^{2,2,7}GTP$) exists in the upstream but not the downstream portion of the 3–4 loop.

We next explored combinations of 1–2 loop sequences with 3–4 loop sequences. Variant 1–2 & 3–4 down is more selective for m^7GTP than the corresponding variant 3–4 down (Figure 4A). Variant 1–2 & 3–4 up (Figure 4B), on the other hand, is less selective than the corresponding variant 3–4 up. Similarly, variant 1–2 & 3–4 loop is less selective than variant 3–4 loop. In all three cases, the changes in cap selectivity caused by substitutions in the 3–4 loop are attenuated by substitutions in the 1–2 loop, causing the proteins to behave more like wt IFE-5.

Based on these findings, we sought the specific amino acid residues in the upper 3–4 loop sequence responsible for increased m^7GTP selectivity. Of several single and

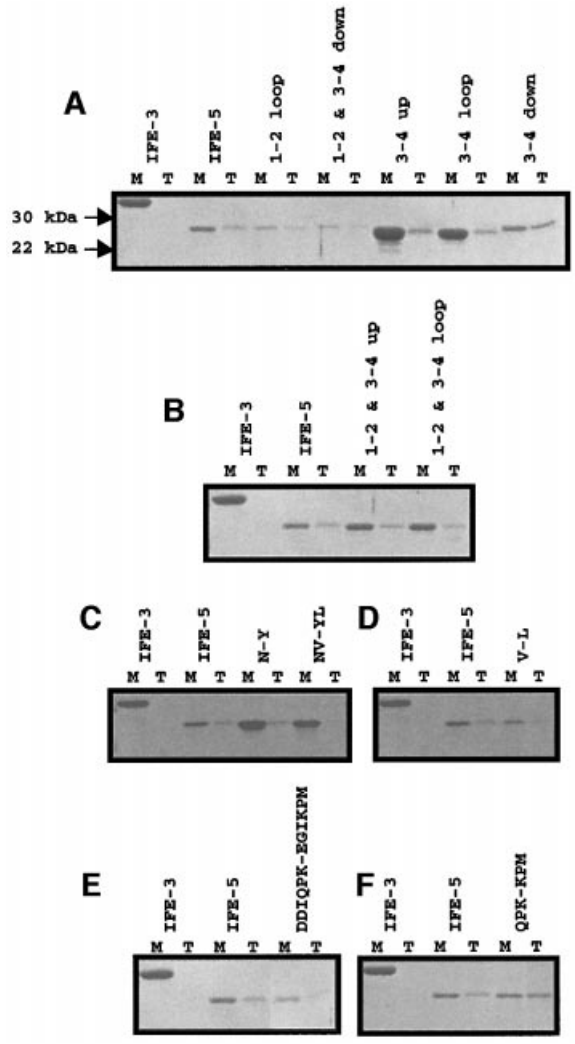

Fig. 4. Qualitative testing of IFE-5 sequence variants using affinity chromatography. *Escherichia coli* was transfected with the indicated expression vectors, and extracts were applied to columns of m^7GTP–Sepharose (M) or $m_3^{2,2,7}GTP$–Sepharose (T). Proteins were eluted with m^7GTP or $m_3^{2,2,7}GTP$, respectively, and analyzed by SDS–PAGE, with Coomassie Blue staining.

double amino acid substitutions, the variant NV-YL produces the highest selectivity: binding to $m_3^{2,2,7}$GTP–Sepharose is nearly undetectable despite robust binding to m^7GTP–Sepharose (Figure 4C and D). The combination of changing both Asn-64 and Val-65, rather than either alone, confers the maximum change in m^7GTP selectivity.

We explored the remaining portion of the 3–4 up region with the variant DDIQPK-EGIKPM (Figure 4E). Despite the fact that binding to both affinity resins is lower than for wt IFE-5, the ratio of binding appears similar to that of wt IFE-5, suggesting no change in selectivity. By contrast, the variant QPK-KPM displays increased binding to $m_3^{2,2,7}$GTP–Sepharose, but the same or even less binding to m^7GTP–Sepharose than IFE-5 (Figure 4F). This indicates that QPK-KPM is even more permissive than IFE-5 for $m_3^{2,2,7}$GTP binding.

A consistent picture emerges from these observations. The 1–2 loop region alone does not affect m^7GTP selectivity. By contrast, the 3–4 loop region is responsible for m^7GTP selectivity, but changes in selectivity are 'damped' in variants combining 1–2 loop and 3–4 loop substitutions. Within the 3–4 loop region, the N-terminal portion (3–4 up) increases selectivity, while the C-terminal portion decreases selectivity. Within the 3–4 up region, simultaneously replacing Asn-64 with Tyr and Val-65 with Leu confers the greatest selectivity, indistinguishable from IFE-3 by this assay. The individual substitutions at positions 64 or 65 do not confer this degree of enhanced selectivity, nor do substitutions in the C-terminal portion of the 3–4 up region. In fact, replacement of the C-terminal one-third of the 3–4 up region has the opposite effect, lowering selectivity. This may account for the observation that exchanging ^{64}NV^{65} (variant NV-YL) increases selectivity more than exchanging ^{64}NVFRDDIQPK^{73} (variant 3–4 up).

Quantitative testing of 1–2 and 3–4 loop IFE-5 variants by fluorescence quenching

To obtain quantitative binding data, we employed the fluorescence-quenching assay with homogeneous IFE proteins. The dissociation constants of the cap analog·protein complexes, K_D, were calculated for both m^7GTP and $m_3^{2,2,7}$GTP titrations (Table I, Experiment 1). The binding of m^7GTP to IFE-3 is 1.3-fold stronger than to IFE-5 (K_D = 0.38 versus 0.50 μM). By contrast, the binding of $m_3^{2,2,7}$GTP is 2.3-fold stronger to IFE-5 than to IFE-3 (K_D = 1.6 versus 3.5 μM). The combined effects of these nucleotide-binding differences is that IFE-3 discriminates in favor of m^7GTP versus $m_3^{2,2,7}$GTP caps by a factor of 9.2, whereas IFE-5 discriminates by a factor of only 3.2 (Table I, K_D ratio).

The quantitative assay confirmed that substitutions of IFE-3 sequences into IFE-5 change m^7GTP selectivity. Variants 1–2 loop, 3–4 loop and 3–4 up are slightly more selective than wt IFE-5 (increase in K_D ratio), whereas 3–4 down is less selective. However, the largest increase is observed with variant NV-YL (K_D ratio = 6.8), which discriminates nearly as well as IFE-3 (K_D ratio = 9.2). The change in selectivity for variant NV-YL occurs because of both an increase in affinity for m^7GTP (1.3-fold) and a decrease in affinity for $m_3^{2,2,7}$GTP (1.7-fold). Interestingly, neither the N-Y nor V-L variants alone show as much increase in K_D ratio as the combination. Some variants are less selective for m^7GTP than wt IFE-5, as reflected in a lower K_D ratio. The largest effect is for variant QPK-KPM, which has a K_D ratio of 1.9 compared with 3.2 for wt IFE-5. This change results from an increase in $m_3^{2,2,7}$GTP affinity rather than a decrease in m^7GTP affinity.

Table I. Dissociation constants (K_D) for m^7GTP and $m_3^{2,2,7}$GTP from various IFE proteins

Protein[a]	Titration buffer[b]	K_D (μM)[c]		K_D ratio[d]
		m^7GTP	$m_3^{2,2,7}$GTP	
Experiment 1				
IFE-3	A_1	0.38 ± 0.03	3.5 ± 0.1	9.2 ± 0.8
IFE-5	A_1	0.50 ± 0.06	1.6 ± 0.1	3.2 ± 0.6
1–2 loop	A_1	0.35 ± 0.02	1.5 ± 0.1	4.3 ± 0.5
3–4 up	A_1	0.43 ± 0.03	1.9 ± 0.1	4.4 ± 0.5
3–4 down	A_1	0.41 ± 0.03	0.81 ± 0.02	2.0 ± 0.2
3–4 loop	A_1	0.46 ± 0.03	1.9 ± 0.1	4.1 ± 0.5
1–2 & 3–4 up	A_1	0.55 ± 0.05	1.5 ± 0.1	2.7 ± 0.4
1–2 & 3–4 down	A_1	0.46 ± 0.02	1.4 ± 0.1	3.0 ± 0.3
1–2 & 3–4 loop	A_1	0.42 ± 0.03	1.1 ± 0.1	2.6 ± 0.4
N-Y	A_1	0.41 ± 0.02	1.4 ± 0.1	3.4 ± 0.4
V-L	A_1	0.43 ± 0.04	2.3 ± 0.1	5.3 ± 0.7
NV-YL	A_1	0.38 ± 0.03	2.6 ± 0.1	6.8 ± 0.8
DDIQPK-EGIKPM	A_1	0.51 ± 0.04	1.6 ± 0.1	3.1 ± 0.4
QPK-KPM	A_1	0.45 ± 0.03	0.85 ± 0.04	1.9 ± 0.2
Experiment 2				
IFE-3	A_0	0.36 ± 0.03	3.5 ± 0.1	9.7 ± 1.1
IFE-5	A_0	0.54 ± 0.07	0.92 ± 0.08	1.7 ± 0.4
3–4 up	A_0	0.47 ± 0.03	0.94 ± 0.03	2.0 ± 0.2
3–4 loop	A_0	0.45 ± 0.04	0.95 ± 0.04	2.1 ± 0.3
NV-YL	A_0	0.68 ± 0.03	1.2 ± 0.1	1.8 ± 0.2
QPK-KPM	A_0	0.57 ± 0.03	1.0 ± 0.1	1.8 ± 0.3
IFE-3	A_{10}	0.39 ± 0.03	3.5 ± 0.1	9.0 ± 0.9
IFE-5	A_{10}	0.48 ± 0.05	1.9 ± 0.1	4.0 ± 0.6
NV-YL	A_{10}	0.32 ± 0.04	2.7 ± 0.1	8.4 ± 1.6

[a]Proteins were dialyzed against buffer A_1 in Experiment 1 and against buffer A_0 in Experiment 2 prior to titration. Buffer A_0 is 50 mM HEPES pH 7.6, 1 mM EDTA, 50 mM KCl, 5% glycerol. Buffer A_1 is buffer A_0 containing 1 mM DTT.
[b]Titrations were carried out in the indicated buffers. Buffer A_{10} is buffer A_0 containing 10 mM DTT.
[c]K_D values were determined by measuring the quenching of intrinsic Trp fluorescence during titration with the indicated cap analogs.
[d]The K_D obtained with $m_3^{2,2,7}$GTP was divided by the K_D obtained with m^7GTP.

Change in selectivity as a function of redox state

A preliminary tertiary structure for IFE-5 revealed a close proximity of Cys-122 and Cys-142, suggesting the possibility of a disulfide bond between them. Also, the two proteins retained on $m_3^{2,2,7}$GTP–Sepharose (IFE-1 and IFE-5) contain Cys residues at four homologous positions, Cys-61, Cys-126, Cys-142 and Cys-185 (using the IFE-5 numbering), that are not present in IFE-3. Conceivably, the tertiary structure of IFE-5 is governed, in part, by disulfide bonds.

We therefore repeated the quantitative determination of K_D values in the absence of reducing agent. Titration of IFE-5 with m^7GTP in buffer A_0, which does not contain dithiothreitol (DTT), reveals a K_D for m^7GTP of 0.54 μM (Table I, Experiment 2). This is statistically the same as the value obtained in buffer A_1, 0.50 μM (Experiment 1). By contrast, titration with $m_3^{2,2,7}$GTP in buffer A_0 yields a

K_D of 0.92 μM, compared with 1.6 μM in buffer A_1. Thus, the affinity of IFE-5 for $m_3^{2,2,7}$GTP increases in the absence of DTT. The overall effect is a 1.9-fold loss of m^7GTP selectivity under more oxidizing conditions (K_D ratio decreases from 3.2 in buffer A_1 to 1.7 in buffer A_0).

For variants 3–4 up and 3–4 loop, the affinity for m^7GTP is statistically the same in the presence or absence of DTT, but the affinity for $m_3^{2,2,7}$GTP increases in buffer A_0. This leads to an overall decrease in m^7GTP selectivity of 2.0- to 2.2-fold for these two variants. The results are even more dramatic for variant NV-YL; the K_D values obtained in buffer A_0 indicate a loss of affinity for m^7GTP and a gain of affinity for $m_3^{2,2,7}$GTP compared with buffer A_1, for a loss of m^7GTP selectivity of 3.8-fold. Overall, the K_D ratios of IFE-5 and all variants tested decreased to approximately the same value in buffer A_0 (average of 2.2 ± 0.6), whereas they ranged as high as 6.8 ± 0.8 in buffer A_1.

We tested the specificity of this effect with several controls. First, the selectivity of IFE-3 is statistically unchanged in buffer A_0 (K_D ratio = 9.7 ± 0.8; Experiment 2) versus buffer A_1 (K_D ratio = 9.2 ± 1.1; Experiment 1). Second, the proteins that had been dialyzed against buffer A_0 were titrated with cap analogs in buffer A_{10} (Experiment 2). The K_D values for IFE-3 are all statistically the same in buffer A_0, A_1 or A_{10}. However, the K_D values and ratios for IFE-5 and variant NV-YL revert to their pre-dialysis values. The fact that these proteins recover their high selectivity for m^7GTP in the presence of DTT shows that subjecting them to air oxidation (dialysis against buffer A_0) does not result in protein denaturation. As a third control, we tested whether redox state influences overall protein stability. IFE-3 and IFE-5, previously dialyzed against buffer A_0, were subjected to progressively higher concentrations of guanidine isothiocyanate (0–2.67 M) in the presence or absence of 10 mM DTT. The proportion of denatured protein was estimated from the ratio of fluorescence emission at 335 nm to that at 355 nm (Hammarström *et al*., 2001). The denaturation curves for both proteins were the same with or without DTT (data not shown), indicating that air oxidation does not affect gross IFE structure.

Since DTT (Cleland, 1964) is a much stronger reducing agent than glutathione (GSH), the predominant reducing agent in the cell, we considered the possibility that the change in cap specificity induced by 1 mM DTT occurs outside the range of normal intracellular reduction potentials. We therefore repeated the titration of IFE-5 with m^7GTP and $m_3^{2,2,7}$GTP at five physiological combinations (Shan *et al*., 1990) of reduced and oxidized (GSSG) glutathione. The K_D ratio was then determined for each redox condition (Figure 5). The results indicated that the affinities of IFE-5 for m^7GTP and $m_3^{2,2,7}$GTP are nearly equal (K_D ratio = 1.3 ± 0.3) in 0 mM GSH and 2.5 mM GSSG. Selectivity increases as the GSH/GSSG ratio increases, reaching a maximum K_D ratio of 2.6 ± 0.4.

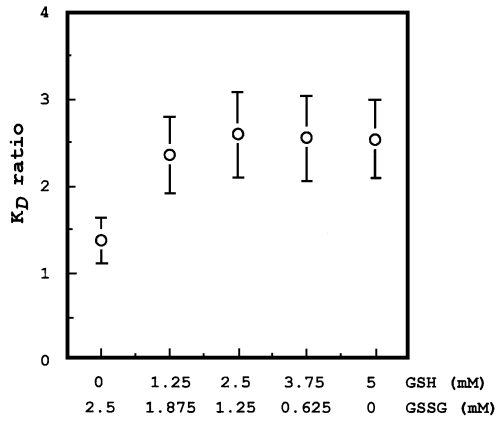

Fig. 5. Change in cap specificity of IFE-5 as a function of reduction potential. The K_D values for dissociation of m^7GTP and $m_3^{2,2,7}$GTP from IFE-5 were determined by fluorescence quenching in buffer A_0 containing the indicated concentrations of reduced (GSH) and oxidized (GSSG) glutathione. The K_D ratios were computed as described in Table I.

Identification of a disulfide bond between Cys-122 and Cys-126

We sought direct evidence that IFE-5 undergoes reversible formation of disulfide bonds. Since the five Cys residues of IFE-5 occur in four different tryptic peptides, we adopted the following strategy. IFE-5 in either the oxidized or reduced states (i.e. dialyzed against either buffer A_0 or A_1) was alkylated with acrylamide, digested with trypsin and the peptides subjected to matrix-assisted laser desorption ionization time-of-flight (MALDI-TOF) mass spectrometry. Peptides containing Cys residues in the sulfhydryl state will have masses that are 71.0 Da greater for every acrylamide moiety incorporated. Peptides containing Cys residues in the disulfide state will not react with acrylamide, and their masses will correspond to the peptide containing a sulfhydryl, an intrastrand disulfide, a mixed disulfide (with another peptide), or some combination of these. By comparing IFE-5 subjected to the same reducing or oxidizing conditions that produced the change in cap specificity, we tested whether the oxidation state of Cys residues could be correlated with the functional change.

Figure 6 shows selected regions of the mass spectra for tryptic peptides from IFE-5 that had been subjected to acrylamidation in either the oxidized (Figure 6A and B) or reduced (Figure 6C and D) states. The peak in Figure 6C at 1580.4 Da is within 0.3 Da of the predicted monoisotopic mass for the doubly acrylamidated peptide ^{117}DMESICGLVCNVR^{129}, which contains Cys-122 and Cys 126. (The peaks at 1581.4, 1582.4 and 1583.4 are isomers of the same peptide containing one, two or three ^{13}C atoms, respectively.) Additional evidence that the cluster of peaks at m/z = 1580.4–1583.4 represents peptide ^{117}DMESICGLVCNVR^{129} comes from a second cluster of peaks at 1596.4–1599.4, representing the same peptides containing Met sulfoxide. The m/z = 1580.4–1583.4 peaks are present in much lower amounts for IFE-5 first dialyzed against buffer A_0 (Figure 6A), indicating that Cys-122 and Cys-126 are predominantly in the disulfide form and therefore unable to react with acrylamide. The absence of a peak at m/z = 1509.4 in Figure 6A, which would have been produced by singly acrylamidated ^{117}DMESICGLVCNVR^{129}, indicates that both Cys-122 and Cys-126 were in the disulfide form at the time of alkylation.

The non-acrylamidated peptide ^{117}DMESICGLVCNVR^{129} has a mass of 1438.6 Da, but a form of this

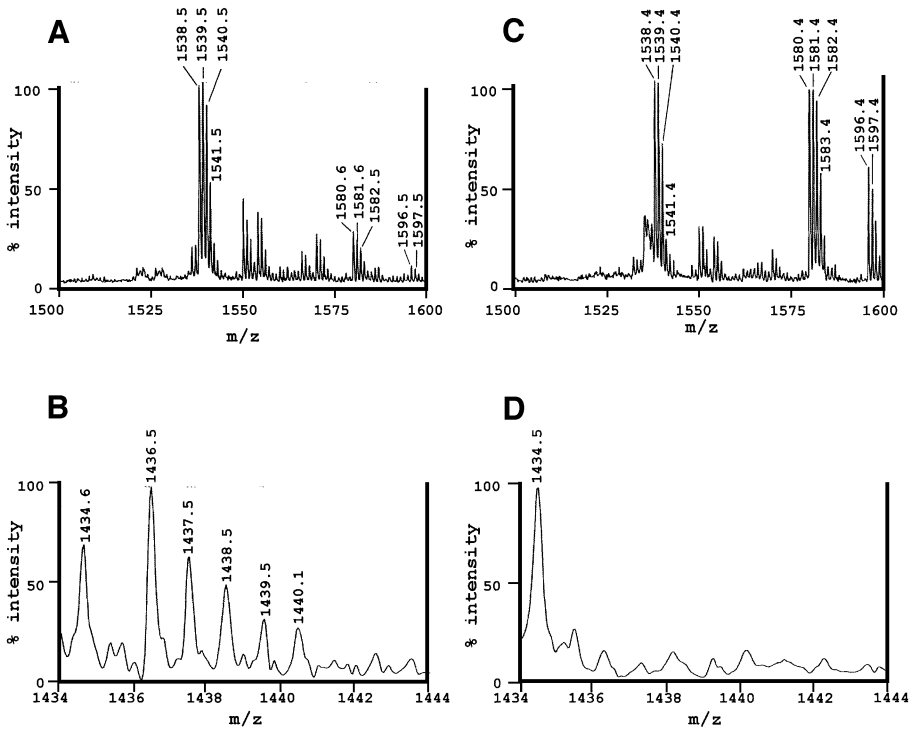

Fig. 6. Determination of the redox state of Cys-122 and Cys-126 in IFE-5 by MALDI-TOF mass spectrometry. Cys residues were alkylated with acrylamide in buffer B containing either no DTT (A and B) or 13 mM DTT (C and D). The proteins were separated by SDS–PAGE and digested with trypsin. (**A** and **C**) Spectra in the *m/z* range of doubly acrylamidated peptide ^{117}DMESICGLVCNVR^{129} (calculated monoisotopic mass 1580.7 Da), indicating that both Cys-122 and 126 are modified by acrylamide under reducing (C) but not oxidizing (A) conditions. (**B** and **D**) Spectra in the *m/z* range of peptide ^{117}DMESICGLVCNVR^{129} containing a disulfide bond between Cys-122 and Cys-126 (calculated monoisotopic mass 1436.6 Da), indicating that this peptide is present under oxidizing (B) but not reducing (D) conditions.

peptide with an intrastrand disulfide between Cys-122 and Cys-126 has a mass of 1436.6. A cluster of isotope-resolved peaks within 0.1 Da of this value, at *m/z* = 1436.5, 1437.5, etc., is observed in the oxidized (Figure 6B) but not the reduced (Figure 6D) IFE-5 sample. Therefore, some or all of the Cys-122 and Cys-126 residues are linked together by an intrastrand disulfide bond in peptide ^{117}DMESICGLVCNVR^{129} in the oxidized form of IFE-5, but this bond is reduced when the protein is dialyzed against buffer A_1.

The protection of Cys-122 and Cys-126 against acrylamidation could also be caused by mixed disulfides with other Cys residues in oxidized IFE-5. We therefore examined the oxidation states of Cys-61 and Cys-142, as determined by acrylamide reactivity. Peaks with *m/z* of the acrylamidated form of peptide ^{35}VYTFNTVPEFWAFYEAILPPSGLNDLCDYNVFR^{67} were observed in equal abundance in oxidized and reduced IFE-5, yet none was observed for the non-acrylamidated form (data not shown), indicating that Cys-61 occurs only in the sulfhydryl form. Similar results were obtained for peptide ^{141}NCNDDDTNMR^{150}, indicating that Cys-142 occurs only in the sulfhydryl form. Unfortunately, Cys-183 is present in a tryptic peptide of <500 Da. This region of the mass spectrum contains too much background noise to yield interpretable results. However, based on the tertiary structure model of IFE-5 (Figure 2), this Cys residue is 12–15 Å from either Cys-122 or Cys-126, so it is unlikely to form mixed disulfide bonds with them.

We obtained similar results using a different alkylating reagent, iodoacetamide, for modification of Cys residues (data not shown). We also obtained mass spectra of tryptic peptides, fractionated by reverse-phase HPLC, from oxidized and reduced IFE-5 without alkylation. A peak corresponding to the intrastrand disulfide form of ^{117}DMESICGLVCNVR^{129} was observed, but no mixed disulfides were found (e.g. between ^{117}DMESICGLVCNVR^{129} and ^{141}NCNDDDTNMR^{150}; data not shown).

The most likely explanation for these results is that Cys-122 and Cys-126 are linked by an intrastrand disulfide bond in oxidized but not reduced IFE-5, whereas Cys-61 and Cys-142 are in the sulfhydryl form in both oxidized and reduced IFE-5. We attempted to obtain further evidence for the involvement of disulfide bonds in cap discrimination by producing IFE-5 variants. However, substituting either Cys-122 or Cys-126 with Ser resulted in proteins that were almost exclusively in the insoluble fraction of the *E.coli* lysate. Although this does allow us to measure cap specificity, it suggests that disulfide bonds may play a role in IFE-5 tertiary structure. Interestingly, IFE-3, which does not undergo a redox-induced change in cap specificity (Table I, Experiment 2), contains a Cys residue (Cys-148) at the equivalent position of Cys-122 in IFE-5, but no equivalent to Cys-126 (Figure 1).

Hypothesis for cap selectivity based on molecular dynamics (MD) modeling

We performed MD simulations to suggest structural hypotheses for the difference in m^7GTP selectivity. Distances were measured between homologous amino acid residues in IFE-3 and IFE-5 during the dynamics trajectories to indicate the dimensions of the cap-binding

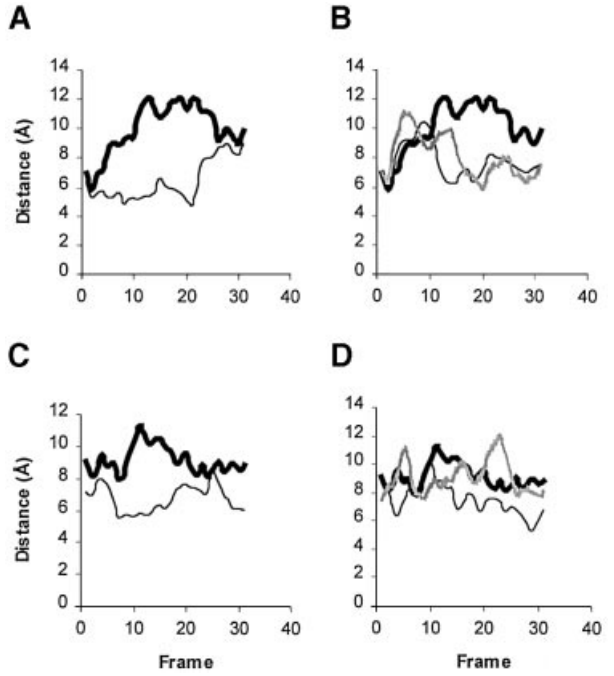

Fig. 7. Dimensions of the cap-binding cavity of IFE-3, IFE-5, and IFE-5 variants NV-YL and N-Y as determined by molecular dynamics simulations. The width of the cavity (**A** and **B**) was measured between the CE2 atom of Trp-51 and the CE2 atom of Trp-97 in IFE-3 (Trp-28 and Trp-74 in IFE-5). The depth of the cavity (**C** and **D**) was measured between the CG atom of Trp-51 and the CZ atom of Tyr-87 in IFE-3 (CG of Trp-28 and ND2 of Asn-64 in IFE-5). Measurements were obtained for each frame (equivalent to 0.3 ps) of the trajectories. In (A) and (C), thin lines represent IFE-3 and thick lines represent IFE-5. In (B) and (D), thick lines represent IFE-5, thin lines represent variant NV-YL and shaded lines represent variant N-Y. The average width and depth dimensions for the simulations were (in Å): 5.61 × 6.53 for IFE-3, 9.39 × 8.84 for IFE-5, 7.34 × 7.23 for NV-YL and 7.56 × 8.87 for N-Y.

pocket (Figure 7). The trajectories revealed that both the width (Figure 7A) and depth (Figure 7C) are greater in IFE-5 (thick lines) than IFE-3 (thin lines) over the course of the simulation. The volume of the binding pocket is determined, in part, by the degree of coordination among Trp-51, Tyr-87, Trp-97 and Trp-164 in IFE-3 (Trp-28, Asn-64, Trp-74 and Trp-138 in IFE-5). In IFE-3, the cap-binding pocket is more tightly circumscribed as a result of π interactions among the aromatic residues.

Amino acid substitutions in IFE-5 that change cap-binding specificity also change the results of MD simulations (Figure 7B and D). The NV-YL variant (thin lines) has a narrower (Figure 7B) and shallower (Figure 7D) binding pocket than IFE-5 (thick lines). This relationship is maintained even with longer simulations (20 ps). By contrast, the depth of the binding pocket of the N-Y variant (Figure 7D, shaded lines) is more like that of IFE-5 than variant NV-YL.

These results suggest a correlation between m^7GTP selectivity and the dimensions of the binding pocket. The pocket is smaller for IFE-3 and the NV-YL variant of IFE-5, which mimics the high m^7GTP selectivity of IFE-3. The pocket is larger for IFE-5 and the N-Y variant of IFE-5, which fails to mimic the m^7GTP selectivity of IFE-3. The measurements of the binding pocket reflect the overall more 'open' structure of the entire IFE-5 protein when compared with IFE-3 (Figure 2). By contrast, variant NV-YL more nearly resembles the 'closed' structure of IFE-3 (Figure 2), particularly in the cap-binding pocket, despite the fact that 99% of its amino acid residues are identical to wt IFE-5.

Discussion

Previous fluorescence-quenching studies have shown that human eIF4E binds m^7G-containing cap analogs 7- to 8-fold more strongly than the equivalent $m_3^{2,2,7}$G-containing analogs (Carberry *et al*., 1990; Wieczorek *et al*., 1999). β-globin mRNA capped with m^7G is translated 6-fold more efficiently in rabbit reticulocyte lysate than the same mRNA capped with $m_3^{2,2,7}$G (Darzynkiewicz *et al*., 1988). Finally, m^7GTP is 17-fold more effective than $m_3^{2,2,7}$GTP for inhibiting translation of rabbit globin mRNA in reticulocyte lysate (Cai *et al*., 1999). We find that IFE-3 binds m^7GTP 9-fold more strongly than $m_3^{2,2,7}$GTP (Table I), indicating that *C.elegans* IFE-3 is similar to the characterized mammalian eIF4Es in cap specificity. By contrast, IFE-5 has only a 3.2-fold preference for m^7GTP over $m_3^{2,2,7}$GTP (Table I).

Several models can be proposed to explain this difference in selectivity. Model 1 postulates that the cap-binding pocket of IFE-3, but not of IFE-5, contains a binding determinant for some feature of m^7GTP that is not shared by $m_3^{2,2,7}$GTP, e.g. the ability to form H-bonds at N2. This model makes several predictions (Table II): (A) the affinity of IFE-3 for m^7GTP is greater than for $m_3^{2,2,7}$GTP, because of the extra binding determinant; (B) the affinities of IFE-5 for m^7GTP and $m_3^{2,2,7}$GTP are approximately equal, because the extra determinant is not present in IFE-5; (C) the affinity of IFE-3 for m^7GTP is greater than the affinity of IFE-5 for m^7GTP, because IFE-5 lacks the extra determinant; and (D) IFE-3 and IFE-5 bind $m_3^{2,2,7}$GTP with nearly the same affinity, because the extra determinant does not affect $m_3^{2,2,7}$GTP. Model 2, a mirror image of Model 1, postulates that IFE-5, but not IFE-3, has a binding determinant for some feature of $m_3^{2,2,7}$GTP that is not shared by m^7GTP, e.g. van der Waals interactions with the N2 methyl groups. The predictions for each of the four interactions are different from Model 1 (Table II, Model 2), but the reasoning is similar. Model 3 postulates that steric hindrance impedes access of $m_3^{2,2,7}$GTP to the cap-binding pocket of IFE-3 but not of IFE-5, whereas m^7GTP can readily enter the binding pocket of both proteins. The set of predictions is different from either of the two previous models (Table II, Model 3). For example, the affinities of IFE-5 for m^7GTP and $m_3^{2,2,7}$GTP (Table II, Model 3, Comparison B) are more similar than those of IFE-3 (Comparison A), because once $m_3^{2,2,7}$GTP is admitted, the binding determinants are the same as for m^7GTP. When the predictions are compared with the actual data (Table II, Found), it is clear that none of the three models agrees with all of the data. We therefore propose a fourth model that combines elements of Models 1 and 3. In Model 4, $m_3^{2,2,7}$GTP is impeded from entering the binding pocket of IFE-3, but not of IFE-5, by steric hindrance. Furthermore, there is a positive determinant for binding m^7GTP, but not $m_3^{2,2,7}$GTP, in both IFE-3 and IFE-5. The prediction of

Table II. Predictions of various models for relative binding of cap analogs to IFE-3 and IFE-5

Comparison of binding	Model 1[a]	Model 2[b]	Model 3[c]	Model 4[d]	Found[e]
(A) IFE-3·m^7GTP versus IFE-3·$m_3^{2,2,7}$GTP	>	≅	>	>	>
(B) IFE-5·m^7GTP versus IFE-5·$m_3^{2,2,7}$GTP	≅	<	≅	>	>
(C) IFE-3·m^7GTP versus IFE-5·m^7GTP	>	≅	≅	≅	≅
(D) IFE-3·$m_3^{2,2,7}$GTP versus IFE-5·$m_3^{2,2,7}$GTP	≅	<	<	<	<

[a]IFE-3, but not IFE-5, contains a positive binding determinant for some feature of m^7GTP that is not shared by $m_3^{2,2,7}$GTP.
[b]IFE-5, but not IFE-3, contains a positive binding determinant for some feature of $m_3^{2,2,7}$GTP that is not shared by m^7GTP.
[c]Steric hindrance impedes the access of $m_3^{2,2,7}$GTP to the cap-binding pocket of IFE-3 but not IFE-5.
[d]There are m^7GTP-specific binding determinants in both IFE-3 and -5, but $m_3^{2,2,7}$GTP is sterically hindered from entering the binding pocket of IFE-3.
[e]Comparison of binding affinities ($1/K_D$) for the interactions shown.

Model 4 for Comparison A is satisfied because of the m^7GTP-specific binding determinant, e.g. Glu-98 of IFE-3, which would form an H-bond with N2 of m^7G. Predictions for Comparisons B and C are satisfied because IFE-5 also contains this determinant (Glu-75). The prediction of Comparison D is satisfied because steric hindrance prevents IFE-3 from admitting $m_3^{2,2,7}$GTP.

The more restricted binding pocket of IFE-3 compared with IFE-5 (Figures 2 and 7) might not admit $m_3^{2,2,7}$GTP because this cap structure is bulkier and more disordered than m^7GTP (Stolarski *et al*., 1996), requiring both a wider Trp spacing to enter the pocket and also a greater depth to accommodate the dimethyl moiety. In addition, the MD simulations indicate that IFE-5 is sufficiently flexible to close the gap between the 'sandwich' Trp residues, allowing the base stacking that provides favorable binding energy (Figure 7A). These results are consistent with the steric hindrance feature of Models 3 and 4, and suggest that Trp spacing impedes $m_3^{2,2,7}$GTP entry in both the mammalian eIF4Es and IFE-3.

All IFE-5 variants that include substitution of Tyr-64 and Leu-65 with Asn and Val, respectively, gain in their discrimination against $m_3^{2,2,7}$GTP, yet maintain a constant affinity for m^7GTP. MD simulations indicate that the substitutions in variant NV-YL are alone sufficient to narrow the inter-Trp stacking distance [Figures 2, IFE-5(NV-YL) and 7B]. This narrowing may be due to interaction of the phenol ring of Tyr-64 with the indole ring of Trp-74 through perpendicular π interactions, restricting the movement of Trp-74 relative to Trp-28 at the opening of the pocket [Figure 2, IFE-5(NV-YL)]. Interestingly, Asn-64 and Val-65 are conserved in all three dual-specific IFEs, but are absent from the two mono-specific IFEs. We constructed molecular models of the other dual-specific IFEs, IFE-1 and IFE-2, and subjected them to MD simulations (data not shown). The models behaved more like IFE-5 than variant NV-YL or IFE-3 in overall dynamics as well as in the dimensions of the cap-binding pocket. We also aligned sequences of all known eIF4Es, from yeasts, insects, plants and vertebrates, and found that positions 64 and 65 are occupied by Asn and Val, respectively, only for IFE-1, -2 and -5. These results suggest that Asn-64 and Val-65 constitute a unique specificity determinant.

No data have been published showing that any of the IFE isoforms discriminate between m^7GTP- and $m_3^{2,2,7}$GTP-capped mRNAs *in vivo*. Rather, we have only shown in the present study and in previous work that these proteins differ in their binding to the free nucleotides or Sepharose-linked forms of the nucleotides. It is, nonetheless, tempting to speculate that, *in vivo*, the more m^7GTP-selective IFE isoforms recruit canonical m^7GTP-capped mRNAs to the ribosome, whereas those IFE isoforms that are more permissive for $m_3^{2,2,7}$GTP recruit *trans*-spliced mRNAs. Because at least some of the IFE proteins differ in tissue distribution (Amiri *et al*., 2001), and because m^7GTP- and $m_3^{2,2,7}$GTP-capped mRNAs are transcribed from different genes (Blumenthal, 1998), the presence of certain combinations of IFE proteins differing in cap specificity may account in part for the particular spectrum of proteins expressed in a given tissue.

Our results also suggest the possibility that mRNA cap-binding selectivity may be regulated by intracellular redox changes in the case of IFE-5 but not IFE-3. In the absence of a thiol reagent, there is both formation of a disulfide bond between Cys-122 and Cys-126 (Figure 6) and a decrease in the m^7GTP selectivity of IFE-5 (Table I; Figure 5). It is conceivable that the formation of this disulfide bond serves as a reversible switch that responds to the redox state of the cell, as has recently been reported for the molecular chaperone Hsp33 (Jakob *et al*., 1999). Such a disulfide bond switch could modulate the recognition of $m_3^{2,2,7}$GTP-containing mRNAs by IFE-1, -2 and -5 *in vivo*, altering the relative translation of *trans*-spliced versus canonical mRNAs.

Materials and methods

Materials

Restriction enzymes and *Pfu* DNA polymerase were obtained from Promega. A DNA ligation kit (version 2) was purchased from Takara Shuzo Co., Ltd. m^7GTP was purchased from Sigma, and m^7GTP–Sepharose from Pharmacia Biotech, Inc. $m_3^{2,2,7}$GTP and $m_3^{2,2,7}$GTP–Sepharose were synthesized (Jankowska *et al*., 1993). Buffer A_0 is 50 mM HEPES, pH 7.6, 1 mM EDTA, 50 mM KCl and 5% glycerol; buffer A_1 is buffer A_0 containing 1 mM DTT; and buffer A_{10} is buffer A_0 containing 10 mM DTT.

Construction of expression vectors for IFE-3, IFE-5 and variant forms of IFE-5

pETife3 and pETife5, encoding IFE-3 and IFE-5, respectively, were prepared as described previously (Keiper *et al*., 2000). A segment between the *Afl*II and *Xho*I sites in pETife3, corresponding to a portion of the 3′-UTR of the transcribed mRNA (372 bp), was deleted to create plasmid pETife3-2, improving the yield of IFE-3. Site-directed mutagenesis of pETife5 was performed using the overlap extension method (Horton *et al*., 1989) to modify sequences between the *Nde*I and *Xho*I restriction sites. The resultant fragment was ligated into the same sites of pET21b. The sequences of all constructs were confirmed at the Iowa State University facility.

Expression, initial characterization and purification of recombinant IFE proteins

Escherichia coli BL21(DE3)pLysS cells were transformed with pETife3-2, pETife5 and mutated forms of pETife5. Cells were cultured in Luria–Bertani medium containing 100 μg/ml ampicillin and 20 μg/ml chloramphenicol at 25°C. Cultures of 100 ml and 2 l were used for analytical and preparative experiments, respectively. When the A_{600} reached 0.5, expression of IFE proteins was induced for 6 h with 50 μM IPTG, after which cells were harvested by centrifugation. Subsequent steps were performed at 4°C. The cells were suspended in 2 ml of buffer A_1 containing 100 μM GTP for analytical experiments (20 ml for preparative experiments), disrupted by sonication and the lysate centrifuged.

For analytical characterization of cap-binding properties, 1 ml of the supernatant was applied to 0.3 ml columns of either m^7GTP– or $m_3^{2,2,7}$GTP–Sepharose equilibrated with buffer A_1. The columns were washed three times with 5 ml portions of buffer A_1, and the bound proteins were eluted with 1.5 ml of either 100 μM m^7GTP or $m_3^{2,2,7}$GTP, respectively, in buffer A_1. Proteins were precipitated by addition of trichloroacetic acid to a final concentration of 10% at 0°C for 30 min, collected by centrifugation, washed twice with 1 ml aliquots of –20°C acetone and dissolved in 50 μl of SDS–PAGE sample buffer. Half of each sample was analyzed by SDS–PAGE using a 15% gel with an acrylamide:*N*,*N*′-bisacrylamide ratio of 29:1.

For fluorescence studies, the cleared *E.coli* lysate was subjected to affinity chromatography on 1 ml columns of m^7GTP–Sepharose as described above. The protein eluted with m^7GTP was further purified to homogeneity on a MonoQ column (Amersham Pharmacia Biotech) and dialyzed against either buffer A_0 or buffer A_1, as indicated in the text. Protein concentrations were estimated by dye binding (Bradford, 1976).

Fluorescence measurements

The affinity of IFE proteins for cap analogs was measured by quenching of intrinsic Trp fluorescence during titration with either m^7GTP or $m_3^{2,2,7}$GTP (Carberry *et al*., 1989; Wieczorek *et al*., 1998). Measurements were performed on a Model 750 Strobe-Master lifetime spectrofluorometer from Photon Technology Inc. (South Brunswick, NJ). The instrument was equipped with an SE-900 steady-state fluorescence option that utilizes a 75 W xenon arc lamp with photon counting detection. All measurements were made in a 5-mm-ID cylindrical quartz cuvette at 25°C using an excitation wavelength of 295 nm, emission wavelength of 348 nm, lamp slit of 2 nm, monochrometer slit of 3 nm and emission slit of 5 nm. Titrations were performed by adding m^7GTP or $m_3^{2,2,7}$GTP to a 300 μl solution containing 1 μM IFE protein in either buffer A_0, A_1 or A_{10}. Fluorescence values were corrected for the dilution of the sample during titration. The contribution of buffer components to overall fluorescence was determined separately and subtracted.

ΔF was calculated from the expression:

$$\Delta F = F_0 - F_a \quad (1)$$

where F_0 is the fluorescence before addition of cap analog and F_a is the fluorescence after each addition. The inner filter effect (Lakowicz, 1999) was corrected using the relationship:

$$F_{corr} = F_{observed} \times \text{antilog}_{10}[(A_{295nm} + A_{348nm})/2] \quad (2)$$

Dissociation constants (K_D) were calculated using the program KaleidaGraph (Version 3.06; Synergy Software, Reading, PA) by non-linear least squares fitting of equation (3):

$$\Delta F/\Delta F_{max} = a/(K_D + a) \quad (3)$$

where a is the cap analog concentration in micromolar and ΔF_{max} is given by the expression:

$$\Delta F_{max} = F_0 - F_{40\ \mu M\ cap\ analog} \quad (4)$$

Chemical modification of Cys residues in IFE-5

IFE-5 was dialyzed against buffer A_0, and 5 μl of a 1 mg/ml solution were diluted into either 45 μl of buffer B_0 (0.5 M Tris–HCl, pH 8.5, 7 M guanidine–HCl, 10 mM EDTA) or buffer B_{13} (buffer B_0 containing 13 mM DTT). The protein was allowed to stand for 2 h at room temperature, and then 2 μl of a 7 M acrylamide solution were added (Sechi and Chait, 1998). After standing for 40 min in the dark at room temperature, the reaction mixture was diluted with 38 μl of deionized H_2O, and protein was precipitated with trichloroacetic acid and separated by SDS–PAGE. The IFE band was visualized by Coomassie Blue staining and excised. In-gel digestion with trypsin and MALDI-TOF mass spectrometric analysis were performed at the LSUHSC-S Research Core Facility as described previously (Bradley *et al*., 2002). A similar procedure was used for alkylation of Cys residues using iodoacetamide (Hirs, 1967).

Molecular modeling

Computational analyses were performed on a Silicon Graphics Indigo^2 workstation with the Insight II software package from Molecular Simulations, Inc. (now Accelrys; San Diego, CA). Tertiary structure models of *C.elegans* IFE-3 and IFE-5 were created by homology modeling (Dwyer, 1996, 2001). The atomic coordinates for mouse eIF4E (Marcotrigiano *et al*., 1997) were kindly provided by Dr Stephen Burley, Rockefeller University, and served as the template for model building. The amino acid sequence of IFE-5 was automatically aligned with that of mouse eIF4E, and adjustments were made to account for gaps or differences in length. Atomic coordinates for structurally conserved regions were assigned, best-fitting loops were selected from the Protein Data Bank, and steric clash was eliminated. In order to model a disulfide bond between Cys-122 and Cys-126 in IFE-5, the segment containing these residues was constructed as a helical turn with the two Cys residues approaching a disulfide bond. These two residues were then fixed in subsequent minimizations and MD simulations to retain their relative positions. The model of IFE-5 was then subjected to energy minimization to convergence. The model of IFE-3 was similarly built.

MD studies of IFE-3, IFE-5 and variants of IFE-5 were carried out as described previously (Dwyer, 2001). Briefly, the AMBER force field was used with a distance-dependent dielectric constant of 4.0 and a non-bond 1–4 scaling factor of 0.5. The time step was 1 fs and the temperature was 310°K. Each run was initiated with 200 iterations of energy minimization (steepest descents algorithm) to resolve structural alterations introduced by amino acid substitutions in variant proteins. MD simulations were conducted for a total of 10–20 ps with 2000 iterations of equilibration, and frames were saved every 300 steps.

Acknowledgements

The authors gratefully acknowledge Drs Stephan Witt, Robert Smith, Tak Yee Aw, and Zbigniew Wieczorek for valuable advice, Clint Beniot and the LSUHSC-S Research Core Facility for conducting mass spectrometry measurements, Tolvert Fowler for MonoQ purification of IFE proteins and Shannon Walls for construction of the plasmid encoding variant 3–4 loop down. This work was supported by Grant GM20818 from the National Institutes of Health and Grant 6 P04A 05517 from The Polish Committee for Scientific Research.

References

Altmann,M., Müller,P.P., Pelletier,J., Sonenberg,N. and Trachsel,H. (1989) A mammalian translation initiation factor can substitute for its yeast homologue *in vivo*. *J. Biol. Chem.*, **264**, 12145–12147.

Amiri,A., Keiper,B.D., Kawasaki,I., Fan,Y., Kohara,Y., Rhoads,R.E. and Strome,S. (2001) An isoform of eIF4E is a component of germ granules and is required for spermatogenesis in *C.elegans*. *Development*, **128**, 3899–3912.

Blumenthal,T. (1998) Gene clusters and polycistronic transcription in eukaryotes. *BioEssays*, **20**, 480–487.

Bradford,M.M. (1976) A rapid and sensitive method for the quantitation of microgram quantities of protein utilizing the principle of protein–dye binding. *Anal. Biochem.*, **72**, 248–254.

Bradley,C.A., Padovan,J.C., Thompson,T.L., Benoit,C.A., Chait,B.T. and Rhoads,R.E. (2002) Mass spectrometric analysis of the N-terminus of translational initiation factor eIF4G-1 reveals novel isoforms. *J. Biol. Chem.*, **277**, 12559–12571.

Browning,K.S., Lax,S.R. and Ravel,J.M. (1987) Identification of two messenger RNA cap binding proteins in wheat germ. *J. Biol. Chem.*, **262**, 11228–11232.

Cai,A., Jankowska-Anyszka,M., Centers,A., Chlebicka,L., Stepinski,J., Stolarski,R., Darzynkiewicz,E. and Rhoads,R.E. (1999) Quantitative assessment of mRNA cap analogs as inhibitors of *in vitro* translation. *Biochemistry*, **38**, 8538–8547.

Carberry,S.E., Rhoads,R.E. and Goss,D.J. (1989) A spectroscopic study of the binding of m^7GTP and m^7GpppG to human protein synthesis initiation factor 4E. *Biochemistry*, **28**, 8078–8083.

Carberry,S.E., Darzynkiewicz,E., Stepinski,J., Tahara,S.M., Rhoads,R.E. and Goss,D.J. (1990) A spectroscopic study of the binding of N-7-

substituted cap analogs to human protein synthesis initiation factor 4E. *Biochemistry*, **29**, 3337–3341.
Cleland,W.W. (1964) Dithiothreitol, a new protective reagent for SH groups. *Biochemistry*, **3**, 480–482.
Darzynkiewicz,E., Stepinski,J., Ekiel,I., Jin,Y., Haber,D., Sijuwade,T. and Tahara,S.M. (1988) β-globin mRNAs capped with m^7G, $m^{2,2}G$, or $m^{2,2,7}G$ differ in intrinsic translation efficiency. *Nucleic Acids Res.*, **16**, 8953–8962.
De Benedetti,A. and Harris,A.L. (1999) eIF4E expression in tumors: its possible role in progression of malignancies. *Int. J. Biochem. Cell Biol.*, **31**, 59–72.
Dwyer,D.S. (1996) Molecular model of interleukin 12 that highlights amino acid sequence homologies with adhesion domains and gastrointestinal peptides. *J. Mol. Graph.*, **14**, 148–157.
Dwyer,D.S. (2001) Model of the 3-D structure of the GLUT3 glucose transporter and molecular dynamics simulation of glucose transport. *Proteins*, **42**, 531–541.
Gao,M.-X., Rychlik,W. and Rhoads,R.E. (1998) Cloning and characterization of human eIF4E genes. *J. Biol. Chem.*, **273**, 4622–4628.
Gorlich,D. and Mattaj,I.W. (1996) Nucleocytoplasmic transport. *Science*, **271**, 1513–1518.
Hamm,J., Darzynkiewicz,E., Tahara,S.M. and Mattaj,I.W. (1990) The trimethylguanosine cap structure of U1 snRNA is a component of a bipartite nuclear targeting signal. *Cell*, **62**, 569–577.
Hammarström,P., Schneider,F. and Kelly,J.W. (2001) *Trans*-suppression of misfolding in an amyloid disease. *Science*, **293**, 2459–2462.
Hershey,J.W.B. and Merrick,W.C. (2000) Pathway and mechanism of initiation of protein synthesis. In Sonenberg,N., Hershey,J.W.B. and Mathews,M.B. (eds), *Translational Control of Gene Expression*. Cold Spring Harbor Laboratory Press, Cold Spring Harbor, NY, pp. 33–88.
Hirs,C.H.W. (1967) Reduction and *S*-carboxymethylation of proteins. *Methods Enzymol.*, **11**, 199–203.
Horton,R.M., Hunt,H.D., Ho,S.N., Pullen,J.K. and Pease,L.R. (1989) Engineering hybrid genes without the use of restriction enzymes: gene splicing by overlap extension. *Gene*, **77**, 61–68.
Huber,J., Cronshagen,U., Koadokura,M., Marshallsay,C., Wada,T., Sekine,M. and Luhrmann,R. (1998) Snurportin1, an m^3G-cap-specific nuclear import receptor with a novel domain structure. *EMBO J.*, **17**, 4114–4126.
Jakob,U., Muse,W., Eser,M. and Bardwell,J.C.A. (1999) Chaperone activity with a redox switch. *Cell*, **96**, 341–352.
Jankowska,M., Temeriusz,A., Stolarski,R. and Darzynkiewicz,E. (1993) Synthesis of $m_2^{2,7}$GTP– and $m_3^{2,2,7}$GTP–Sepharose 4B: new affinity resins for isolation of cap binding proteins. *Collect. Czech. Chem. Commun.*, **58**, 132–135.
Jankowska-Anyszka,M., Lamphear,B.J., Aamodt,E.J., Harrington,T., Darzynkiewicz,E., Stolarski,R. and Rhoads,R.E. (1998) Multiple isoforms of eukaryotic protein synthesis initiation factor 4E in *C.elegans* can distinguish between mono- and trimethylated mRNA cap structures. *J. Biol. Chem.*, **273**, 10538–10542.
Keiper,B.D., Lamphear,B.J., Deshpande,A.M., Jankowska-Anyszka,M., Aamodt,E.J., Blumenthal,T. and Rhoads,R.E. (2000) Functional characterization of five eIF4E isoforms in *Caenorhabditis elegans*. *J. Biol. Chem.*, **275**, 10590–10596.
Lakowicz,J.R. (1999) *Principles of Fluorescence Spectroscopy*. Kluwer Academic/Plenum, New York, NY.
Liou,R.F. and Blumenthal,T. (1990) *Trans*-spliced *Caenorhabditis elegans* messenger RNAs retain trimethylguanosine caps. *Mol. Cell. Biol.*, **10**, 1764–1768.
Marcotrigiano,J., Gingras,A.-C., Sonenberg,N. and Burley,S.K. (1997) Cocrystal structure of the messenger RNA 5′ cap-binding protein (eIF4E) bound to 7-methyl-GDP. *Cell*, **89**, 951–961.
Matsuo,H., Li,H., McGuire,A.M., Fletcher,C.M., Gingras,A.-C., Sonenberg,N. and Wagner,G. (1997) Structure of translation factor eIF4E bound to m^7GDP and interaction with 4E-binding protein. *Nat. Struct. Biol.*, **4**, 717–724.
Mattaj,I.W. (1986) Cap trimethylation of U snRNA is cytoplasmic and dependent on U snRNP protein binding. *Cell*, **46**, 905–911.
Myers,E.W. *et al.* (2000) A whole-genome assembly of *Drosophila*. *Science*, **287**, 2196–2204.
Rychlik,W., Domier,L.L., Gardner,P.R., Hellmann,G.M. and Rhoads, R.E. (1987) Amino acid sequence of the mRNA cap-binding protein from human tissues. *Proc. Natl Acad. Sci. USA*, **84**, 945–949.
Sechi,S. and Chait,B.T. (1998) Modification of cysteine residues by alkylation. A tool in peptide mapping and protein identification. *Anal. Chem.*, **70**, 5150–5158.
Shan,X., Aw,T.Y. and Jones,D.P. (1990) Glutathione-dependent protection against oxidative injury. *Pharmacol. Ther.*, **47**, 61–71.
Stolarski,R. *et al.* (1996) ^{1}H-NMR studies on association of mRNA cap-analogues with tryptophan-containing peptides. *Biochim. Biophys. Acta*, **1293**, 97–105.
vanDoren,K. and Hirsh,D. (1990) mRNAs that mature through *trans*-splicing in *Caenorhabditis elegans* have a trimethylguanosine cap at their 5-termini. *Mol. Cell. Biol.*, **10**, 1769–1772.
Vandenberghe,A.E., Meedel,T.H. and Hastings,K.E. (2001) mRNA 5′-leader *trans*-splicing in the chordates. *Genes Dev.*, **15**, 294–303.
Varani,G. (1997) A cap for all occasions. *Structure*, **5**, 855–858.
Wakiyama,M., Saigoh,M., Shiokawa,K. and Miura,K. (1995) mRNA encoding the translation initiation factor eIF-4E is expressed early in *Xenopus* embyrogenesis. *FEBS Lett.*, **360**, 191–193.
Wieczorek,Z., Darzynkiewicz,E. and Lonnberg,H. (1998) A fluorescence spectroscopic study on the binding of mRNA 5′-cap-analogs to human translation initiation factor eIF4E: a critical evaluation of the source of error. *J. Photochem. Photobiol. B*, **43**, 158–163.
Wieczorek,Z. *et al.* (1999) Fluorescence studies on association of human translation initiation factor eIF4E with mRNA cap-analogues. *Z. Naturforsch. [C]*, **54**, 278–284.
Zorio,D.A.R., Cheng,N.S.N., Blumenthal,T. and Spieth,J. (1994) Operons as a common form of chromosomal organization in *C.elegans*. *Nature*, **372**, 270–272.

Received March 6, 2002; revised July 16, 2002; accepted July 17, 2002